Characterising the rheology of lamellar gel networks with optical coherence tomography velocimetry

DOI:
10.1122/8.0000599

Document Version
Accepted author manuscript

Characterising the rheology of lamellar gel networks with optical coherence tomography velocimetry

Owen Watts Moore [a, b], Thomas Waigh [a, b, *], Cesar Mendoza [c], Adam Kowalski [c]

[a] Biological Physics, School of Physics and Astronomy, University of Manchester, Oxford Road, Manchester, M13 9PL, UK

[b] Photon Science Institute, University of Manchester, Oxford Road, Manchester, M13 9PL, UK

[c] Unilever Research & Development, Port Sunlight Laboratory, Quarry Road East, Bebington, Wirral CH63 3JW, UK

*To whom correspondence should be addressed: t.a.waigh@manchester.ac.uk

Abstract

Lamellar gel networks based on mixtures of cetostearyl alcohol and a cationic surfactant, cetyl-trimethylammonium chloride (CTAC), were studied using a combination of rheometry and optical coherence tomography (OCT) velocimetry. Experiments were conducted in a stress-controlled rheometer with a parallel plate geometry. Each formulation was found to exhibit a yield stress and thixotropy. The shear start-up behaviour in response to a constant stress was directly observed using OCT velocimetry. Close to the yield stress, the velocity had a power law behaviour with time after an initial period of transience. At larger stresses, the velocity undergoes two successive increases in power law scaling with time. When sheared at low, constant, shear rates 1-5 s^{-1}, the fluids exhibit plug flow with strong wall slip at both rheometer plates. At rates of 10-150 s^{-1}, the fluids separate into a distinctive three shear band morphology while wall slip reduces. These rheological properties can be explained by a multilamellar vesicle (MLV) to planar lamellae transition.

1 Introduction

Lamellar gel networks (LGNs) are multiphase structures with at least three components. These are a lamellar gel, known as the L_β phase, consisting of bilayers of surfactants and fatty alcohols separated by water, bulk water, and crystals of hydrated fatty alcohol, sometimes accompanied by oil stabilised by a surfactant monolayer [1–3]. Surfactants are said to be amphiphilic, in that they have distinct lyophilic and hydrophilic regions of the molecule. These typically take the form of a lyophilic long carbon chain attached to a hydrophilic head group [4]. In the L_β phase, the surfactants pack in a hexagonal structure, with a high degree of order in the carbon chain. The L_β phase can exist either as large, effectively infinite sheets of planar lamellae or as spherical multilamellar vesicles (MLVs) [1]. If the L_β phase is heated past a critical melting point, this order will disappear leading to the lamellar liquid crystal, or L_α, phase. In this phase, most of the interlamellar water is expelled to the bulk, reducing the bilayer thickness which, along with the reduced rigidity due to its newfound disorder, results in the solution being able to move as a liquid [1,5,6]. A property of LGNs is that they usually behave like elastic solids when at rest. This applies up to a yield stress, above which the material will readily flow [1]. This gel-like behaviour doesn't hold true for all lamellar structures. If a material consisted of aligned lamellae, the layers would easily flow over each other when sheared and it would act as a viscous fluid [7]. If instead, the fluid has domains of connected lamellae oriented in random directions or the lamellar bilayers can curve, forming MLVs, the rigidity of the bilayers will allow the fluid to resist small stresses and form a gel-like substance [1,7,8].

LGNs have become ubiquitous in the cosmetics industry for a variety of reasons. They have favourable stability to phase separation when compared with emulsions and other colloidal systems and a creamy texture. The stability comes from their interconnected structure and the yield stress behaviour makes them perfect for tubes or tubs of product [1]. As yield stress is such a useful property for consumer products, fluids exhibiting this behaviour are exceedingly common [9]. There has been some debate as to whether yield stress fluids exist or whether the transition is just one from a very large, but not infinite, viscosity to another, smaller, viscosity, beginning with Barnes and Walters' 1985 paper 'The Yield Stress Myth' [10]. Whether this is the case or not is somewhat immaterial in the context of an experiment where flows below the yield stress are unobservable. Yield stress fluids are often thixotropic, that is their viscosity decreases with time in response to a constant stress. As a result, the yield stress is dependent on the fluid's shear history [9,11]. This history dependence means that the yield stress can't be understood as a material constant and the fluid can even undergo delayed yielding where it takes a certain amount of time at a constant stress before the fluid yields [12]. The time-dependent nature of the yield stress led Coussot et al. (2002) [11] to link it to the underlying mechanisms of thixotropy. Thixotropy is often modelled based on a local structural parameter to quantify how interconnected a fluid is [13–15]. Møller, et al. (2006) [9] introduced a model linking the yield stress to thixotropy using a similar approach where the local parameters decrease in response to a stress, resulting in microscopic deformations and eventual yielding. Positive as these properties may be for consumer satisfaction, they throw up certain difficulties in studying the rheology of gel networks through standard rheometry. For example, the fragility of the structures makes the linear viscoelastic regime very small. Even loading a sample into the rheometer can break structures in a way that is hard to control, making repeatability difficult to achieve [16–18]. Lamellar gel networks also exhibit nonlinear flows, including wall slip and shear banding, [19] at a large range of shear rates. Shear banding is another phenomenon that occurs in a wide range of complex fluids. It has been observed in wormlike micelles [20–22], polymers [23–25], lamellar structures [26–29] and soft glassy materials [30]. The classic understanding of shear bands is as a transitional regime when the microstructure of the fluid is reorganised by flow [20]. This is often evidenced by a stress plateau in the flow curve bounded by two critical shear rates, $\dot{\gamma}_1$ and $\dot{\gamma}_2$. Between those critical values, there will be two bands in the fluid separated in the direction of the velocity gradient, one sheared at $\dot{\gamma}_1$ and the other at $\dot{\gamma}_2$. In such situations, a simple lever rule is often applied to link the applied shear rate to the real rates in the fluid:

$$\dot{\gamma} = f\dot{\gamma}_1 + (1-f)\dot{\gamma}_2. \quad (1)$$

The relative proportions of the fluid at each shear rate are given by f and $1-f$, the values of which change as the imposed shear rate moves from $\dot{\gamma}_1$ to $\dot{\gamma}_2$. This rule is dependent on the no slip condition [20] and is often found to be broken, especially in wormlike micelles [31–33].

The shear-dependent microstructural transition responsible for shear banding in lamellar fluids is from lamellae to MLVs [28,34]. At low shear rates, the layers will align with their normal parallel to the direction of the velocity gradient. This stage is typified by the presence of many defects in the structure. At intermediate rates, the bilayers form MLVs, the size of which varies as the inverse square of the shear rate and exists in the range <10 μm. The final stage is again aligned with very few defects [35,36]. The MLVs are then resistant to gentle deformation and often stable on the time scale of days to months [35,37,38]. A regime intermediate between MLVs and the high-rate aligned phase also exists where the MLVs form a hexagonal lattice and flow by sliding over each other in layers [39]. The presence of MLVs is also associated with strong wall slip, a feature not present in the aligned regimes [26].

Nonlinear effects like slip and shear banding make standard rheometry measurements unreliable as they record the average response of a fluid assuming homogeneity of flow. Additional techniques to measure the local velocity can be used to help fully characterise the rheological behaviour of this class of fluid. Such techniques include particle imaging velocimetry [19,23], ultrasound [27,33,40,41], rheo-NMR [26,30,32,33,42,43], dynamic light scattering [22,28,34], and optical coherence tomography (OCT) velocimetry [25,44,45]. In this paper, we combine rheometry and OCT velocimetry to characterise the rheology of a lamellar gel network based on a cationic surfactant, cetyl-trimethylammonium chloride (CTAC). OCT is used in a shear rheometer to make time-averaged velocity profiles and transient velocity measurements at a fixed position in the rheometer gap. To our knowledge, this is the first time the latter measurements have been performed.

2 Methods

2.1 Samples

The LGNs used in this paper are made from CTAC, deminearlised water, ceto-stearyl alcohol, a salt in the form of versene Na_2 crystals and a preservative, Kathon CG. These occur in various quantities depending on the specific formulation. The three formulations studied in this paper have a 2:1, 3:1 and 6:1 molar ratio of CTAC to ceto-stearyl alcohol and a solid content of 5%. The samples were provided by Unilever and produced according to methods generally disclosed by Casugbo et al. (2014) in a patent [46] and also by Cunningham et al. (2021) [47].

2.2 Rheometry

In all rheometry experiments, a Bohlin Gemini rheometer was used in a parallel plate geometry. The upper plate is made from clear Perspex, while the lower plate is glass. These facilitate the use of the rheometer with an OCT velocimetry apparatus. The lower plate is held at a temperature of 20.5°C by a water-cooling system that supplies water to the plate via pipes, while a cover is placed over the fluid to reduce the impact of evaporation from the edge. The gap was held at 500 μm in every run. Several experiments where then performed, the first of which records how the instantaneous viscosity changes with time in response to a steady shear rate. This was followed by a step down in shear rate, where a constant rate was applied to the fluid for 500 s before being removed entirely. The shear stress was recorded throughout the initial 500 s and then for 500 s more after the removal of the driving force. Finally, a creep-recovery test was performed where a constant stress was applied for 1000 s before being removed for 600 s while the strain response was recorded.

To ensure that each sample had as close to an identical shear history as possible to reduce the effects of thixotropic memory on the results, a pre-shearing protocol was followed. The stress in the sample plateaus when it is sheared at a constant rate. The initial value for pre-shearing was taken to be approximately three times this value when the samples were sheared at 1 s^{-1}. In the case of the 2:1 sample, this was 16.5 Pa and in the cases of the 3:1 and 6:1 samples, this was 15 Pa. This stress was applied for 100 s followed by 300 s of rest.

2.3 OCT velocimetry

OCT is an optical imaging technique first developed by Huang et al. in 1991 [48]. It uses near infrared light from a source with a broad bandwidth and short coherence length, l_c, in an interferometer [49]. The light is split between a sample and a reference mirror, scattered from each and is then recombined on a

detector. If the two beams remain coherent and interfere, they will create a signal from which depth information about the sample can be extracted. This will only be the case if the optical paths travelled by each are within l_c of each other. Precise depths within the sample can therefore be chosen for analysis by moving the position of the reference mirror. This reduces the impact of multiple scattering as light from other paths will not contribute to the signal, allowing opaque materials to be studied [49]. OCT has found most of its applications in medical settings and is widely used by ophthalmologists as a non-invasive technique for imaging the eye [49]. OCT devices can be adapted to measure the Doppler shift in the frequency of the light in the sample arm due to sample movement [50,51]. This has more recently led to the use of OCT velocimetry as a valuable tool to probe the rheology of complex fluids e.g. for opaque fluids in which particle imaging velocimetry is impossible. A further advantage is that opaque fluids normally have sufficient speckle contrast that they do not need to be seeded with probe spheres. OCT velocimetry has been used to identify phenomena such as shear banding, [25] wall slip, [44] and elastic turbulence [52] and allows the velocities of 3.4 pL volumes within opaque lamellar gels to be measured under shear [45].

The OCT apparatus we use is a fibre-based Mach-Zehnder interferometer as described by Malm et al. (2014) [44]. A schematic diagram is shown in figure 1. The light source is a Covega superluminescent diode (SLD), centred at 1310 nm with a bandwidth of 65 nm and longitudinal coherence length of 9 µm. The light

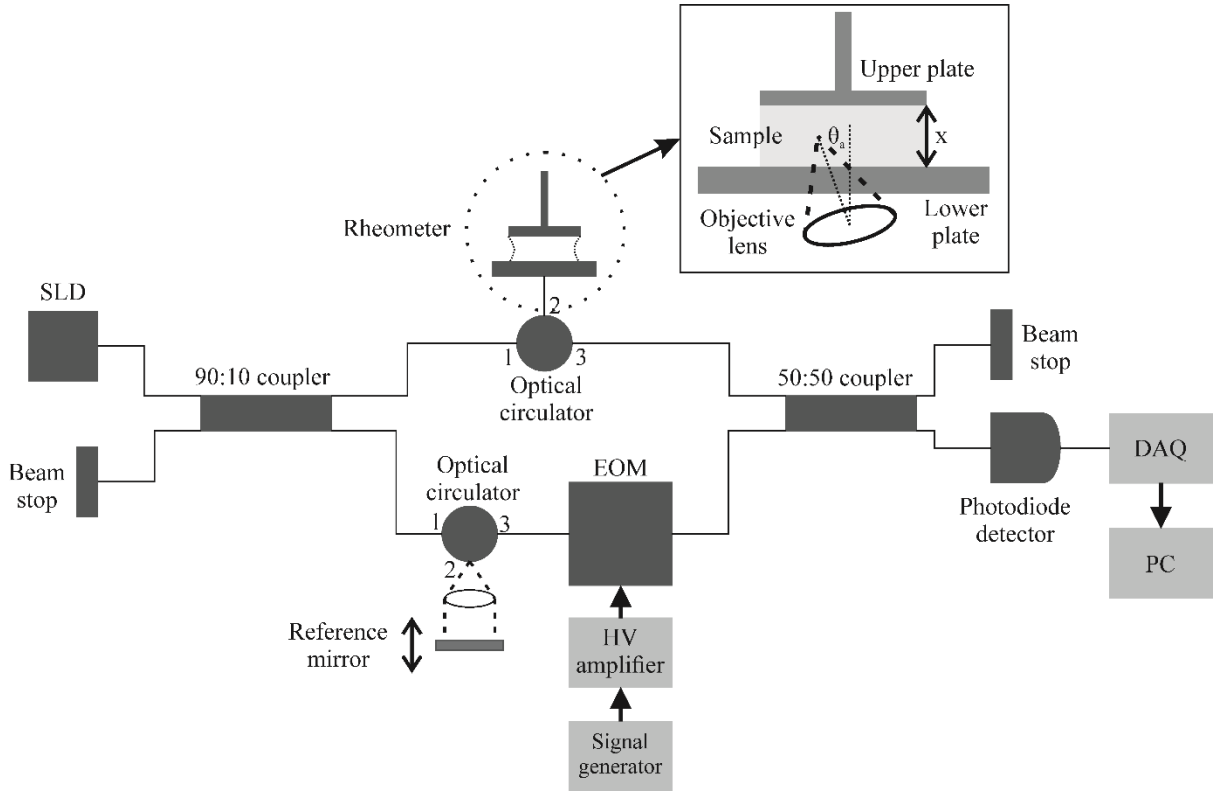

Figure 1. Schematic diagram of the OCT setup used in this study. The lines connecting each optical component represent single-mode optical fibres. The three-port optical circulators direct light that enters port 1 to exit at port 2 and light that enters port 2 to exit port 3. The EOM is driven by a signal generator connected to a high-voltage (HV) amplifier. A close-up of the rheometer is shown in the inset. The objective lens is held at an angle, $\theta_a = 13°$, to the normal of the rheometer plate to prevent backscatter and the gap between the rheometer plates is $x = 500\ \mu m$.

is split by a 90:10 optical coupler, sending 10% to the reference mirror and Thorlabs electro-optic phase modulator (EOM). The reference mirror is mounted on a motorised stage that can be controlled manually or remotely via a LabVIEW program. The EOM is required to probe small velocities as it allows the Doppler signal to be moved by a carrier modulation signal, in these experiments chosen to be either 10 kHz or 20 kHz depending on the Doppler frequency, out of a region of low frequency noise. The modulated signal is then filtered and demodulated to retrieve the Doppler peak in its original position. The other 90% of the source is directed to a specially adapted Bohlin Gemini Mini rheometer with a glass lower plate. The lens at the rheometer is angled at 13° to the normal to the plate and a flat, clear Perspex upper plate with a diameter of 40 mm is used to prevent unwanted back reflection. Light from each arm in then recombined in the coupler before being sent to a photodiode detector.

The majority of medical applications use Fourier domain OCT (FDOCT), rather than the time domain system used in our apparatus. This is because its improved SNR and the lack of a need for a depth scan make it more suited to high resolution imaging [49,53–55]. In this study, time domain OCT (TDOCT) is preferred due to its robustness to low SNR conditions and sensitivity to faster dynamics (set by the data acquisition card) [44].

Two types of measurement were made using OCT velocimetry. The first involved shearing the fluids at constant stresses to investigate the shear start-up behaviour. Measurements of how the velocity varied with time at a constant position in the centre of the rheometer gap were made. This was repeated three times to produce an average result. The second method was shearing the fluid at constant rates ranging from 1 s^{-1} to 150 s^{-1}. The reference mirror was then shifted in 20 micron increments to measure the velocity throughout the fluid and produce a velocity profile. It takes approximately two minutes for a full velocity profile to be produced and three profiles were made from a single sample over periods of approximately 600 s. This procedure was repeated with three samples of each fluid. Each time a set of data was recorded, the rheometer plates were cleared, and the fluid was replaced to reduce the impact of the thixotropic memory of the fluid on results and the same pre-shear routine as described for the rheometry experiments was followed to aid repeatability.

3 Results and discussion

3.1 Rheometry

Figures 2(a-c) show how the viscosity changes with time at various constant shear rates for each of the formulations studied. Shear thinning is an exceedingly common response to shear in complex fluids and can have many different origins [17,56,57]. In this case it is likely to represent a transition from a state of MLVs to aligned lamellar sheets as found by Oliviero et al. (2003) [38]. In all cases, the viscosity follows power law relationships in time of the form $\eta \propto t^{\beta}$, where η is the viscosity, t is the time and β is the exponent. This suggests the processes responsible for the time-dependent viscosity behaviour exhibit a broad range of relaxation times following power law probability distributions[58–60]. In the case of the 2:1 formulation, this is best formulated by two power laws, one each for short ($t \lesssim 100$ s) and long times. Looking at the exponent for the long-time power laws, the magnitude increases with shear rate to a plateau and decreases with increasing surfactant ratio, as can be seen in figure 2(d). At 1 s^{-1} and 5 s^{-1} the power law exponents show a small plateau. The minimum magnitude is with the 1 s^{-1} case in the 6:1 formulation with β = -0.036 ± 0.004 and the maximum is the 1 s^{-1} case in the 2:1 formulation with β = -0.075 ± 0.003. The high-rate plateau comes at $\beta = -0.21 \pm 0.03$, $\beta = -0.136 \pm 0.009$ and $\beta = -0.120 \pm 0.005$ for the 2:1, 3:1 and 6:1 formulations respectively.

Imposing a step down in shear rate can help to determine whether a fluid is thixotropic, viscoelastic or a combination of the two [57]. The stress response of a purely viscoelastic fluid would be to monotonically decrease from an upper value. A purely thixotropic fluid would instantaneously drop to a lower stress before increasing slowly to a steady state level. A fluid showing both viscoelasticity and thixotropy takes time to reach its stress minimum before increasing slowly as in the thixotropic case [57]. The stress responses of our fluids to a step down from a shear rate of 1 s^{-1}, 10 s^{-1} or 100 s^{-1} to a rate of 0.1 s^{-1} are shown in figures 3 (a) - (c). In each figure, the decrease to a stress minimum after the step occurs after a very short time, most closely resembling a purely thixotropic response. The pre-step behaviour can also help us understand the nature of the fluid, as described by Larson and Wei (2019) [17]. The stress response of a purely viscoelastic fluid to a sudden increase in shear rate is to increase to an asymptotic value, while

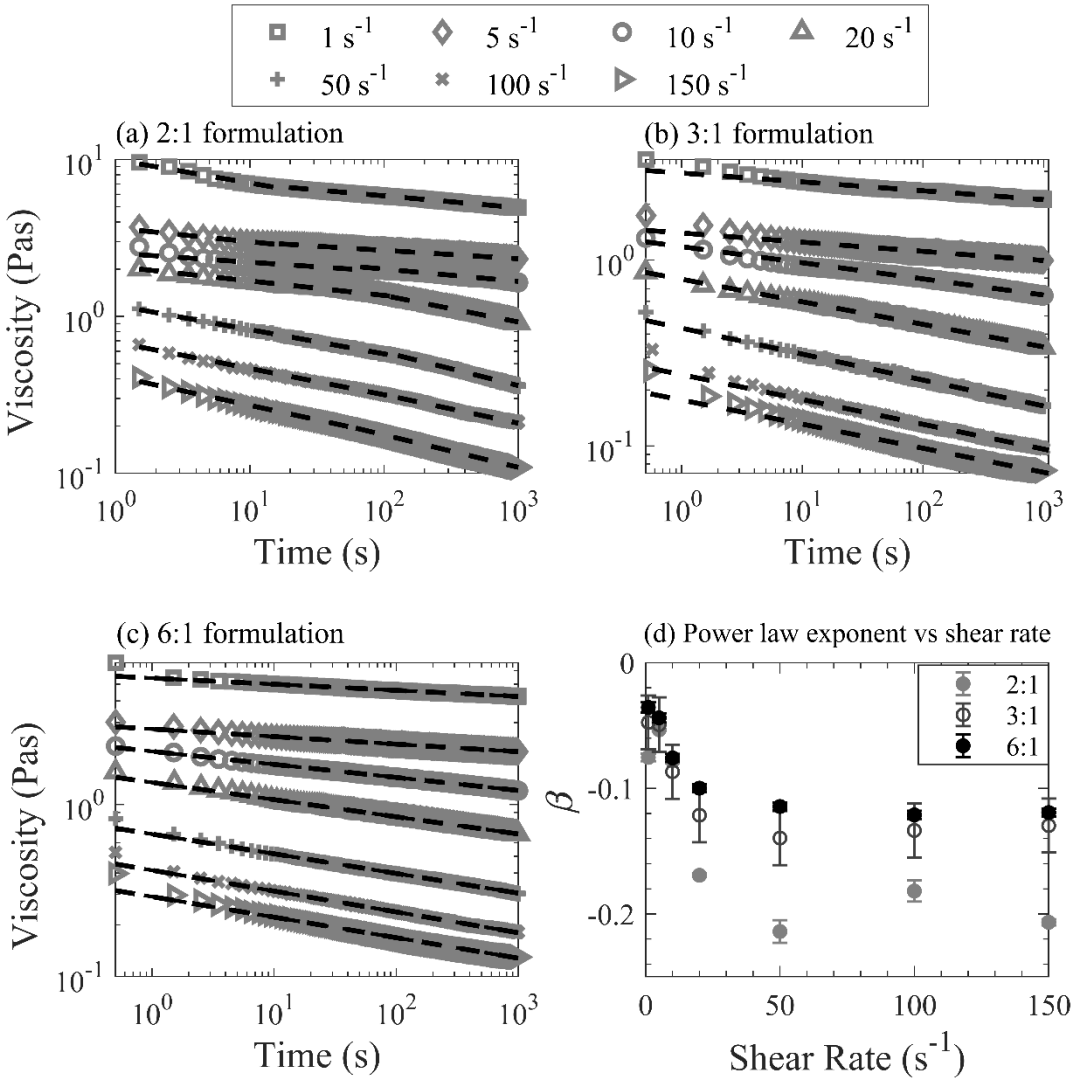

Figure 2. Plots of viscosity vs time for formulations of a lamellar gel network with ratios of CTAC:ceto-stearyl alcohol of (a) 2:1, (b) 3:1 and (c) 6:1 at constant shear rates. At all rates, the fluid shows shear thinning behaviour without reaching the steady state in the timeframe of the experiment. The dashed lines show power law fittings of the form $\eta \propto t^{\beta}$. How the exponent, β, varies with the shear rate for each formulation is shown in (d).

one that exhibits viscoelastic aging will increase to a maximum before decreasing somewhat. A thixotropic fluid will instead start at a maximum stress value, corresponding to the shear rate imposed, before gradually decreasing. This final category describes the behaviour of our fluids, again pointing to thixotropy.

Creep-recovery experiments can show whether, and to what extent, the working fluid exhibits elasticity. On removal of the stress, if strain is recovered, then the fluid must have elasticity as it moves back to some earlier position. Figure 4 shows the creep-recovery data for our fluids. In each case, there is a clear bifurcation in the strain response that occurs between 0.5 Pa and 7 Pa in the case of the 2:1 formulation, 3 Pa and 5 Pa for 3:1 and 1 Pa and 4 Pa for 6:1. Before this transition, some of the strain is recovered once the stress has been removed showing that the fluid exhibits elasticity. After the transition, the fluid loses

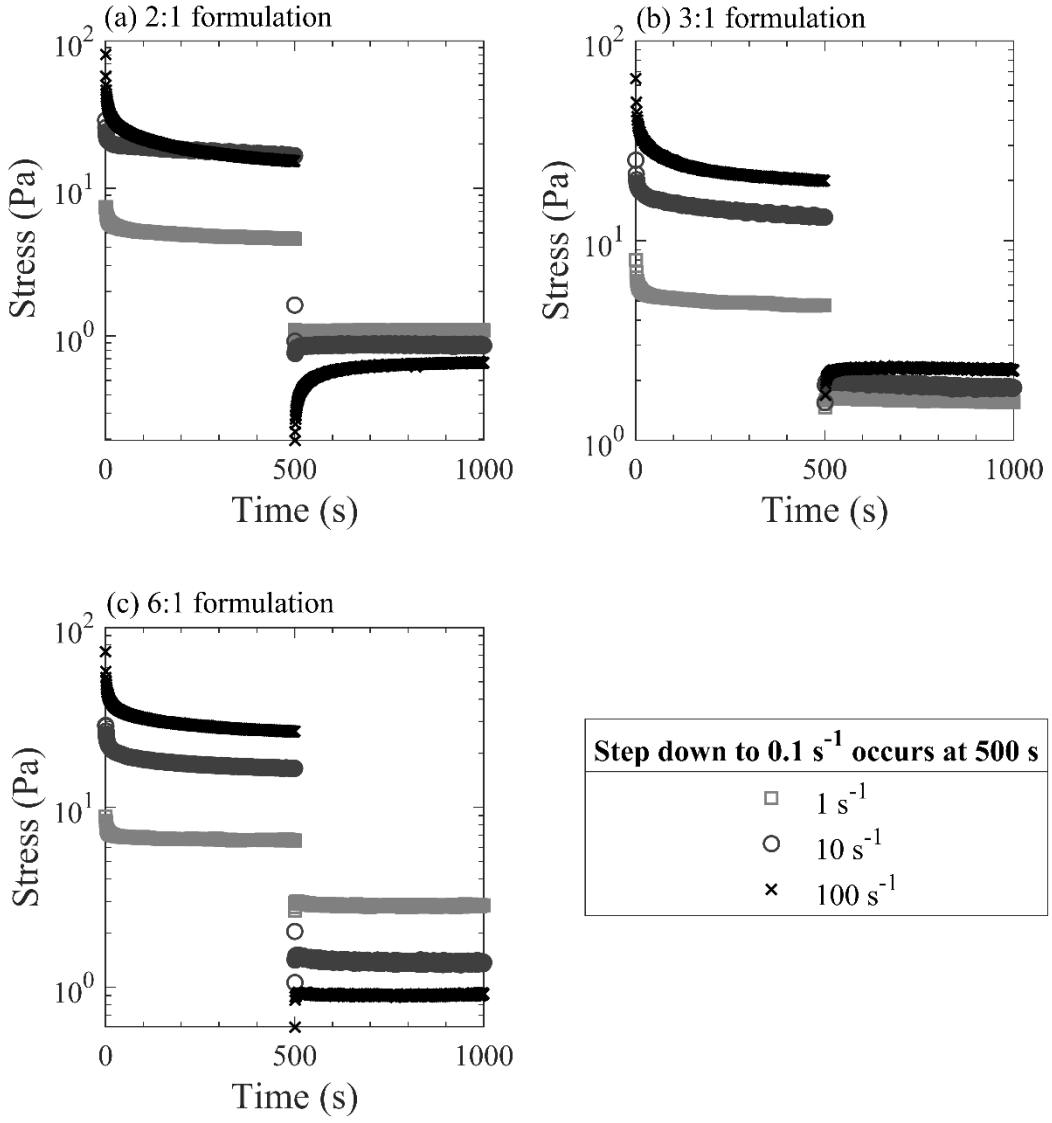

Figure 3. Plots of shear stress against time in response to a step down in shear rate from 100 s^{-1}, 10 s^{-1} and 1 s^{-1} to 0.1 s^{-1} for (a), the 2:1 sample, (b), the 3:1 sample and (c), the 6:1 sample. In all cases, the fluid appears to be thixotropic.

any strain recovery, appearing to act as a viscous fluid. When viewed with OCT, as seen in figure 5, this transition is associated with the onset of motion in the bulk of the fluid and is an expression of a static yield stress in the fluid. In the region between each type of behaviour, the fluids are so sensitive to their shear history that they may fall on either side of the bifurcation on a given experiment. They might even experience delayed yielding after a stress has been applied for a period of time, making reproducibility impossible. On either side of the bifurcation, the creep behaviour can be modelled by a power law. Such fits are included as dashed lines in figure 4. In the pre-yield region, the power laws followed vary between

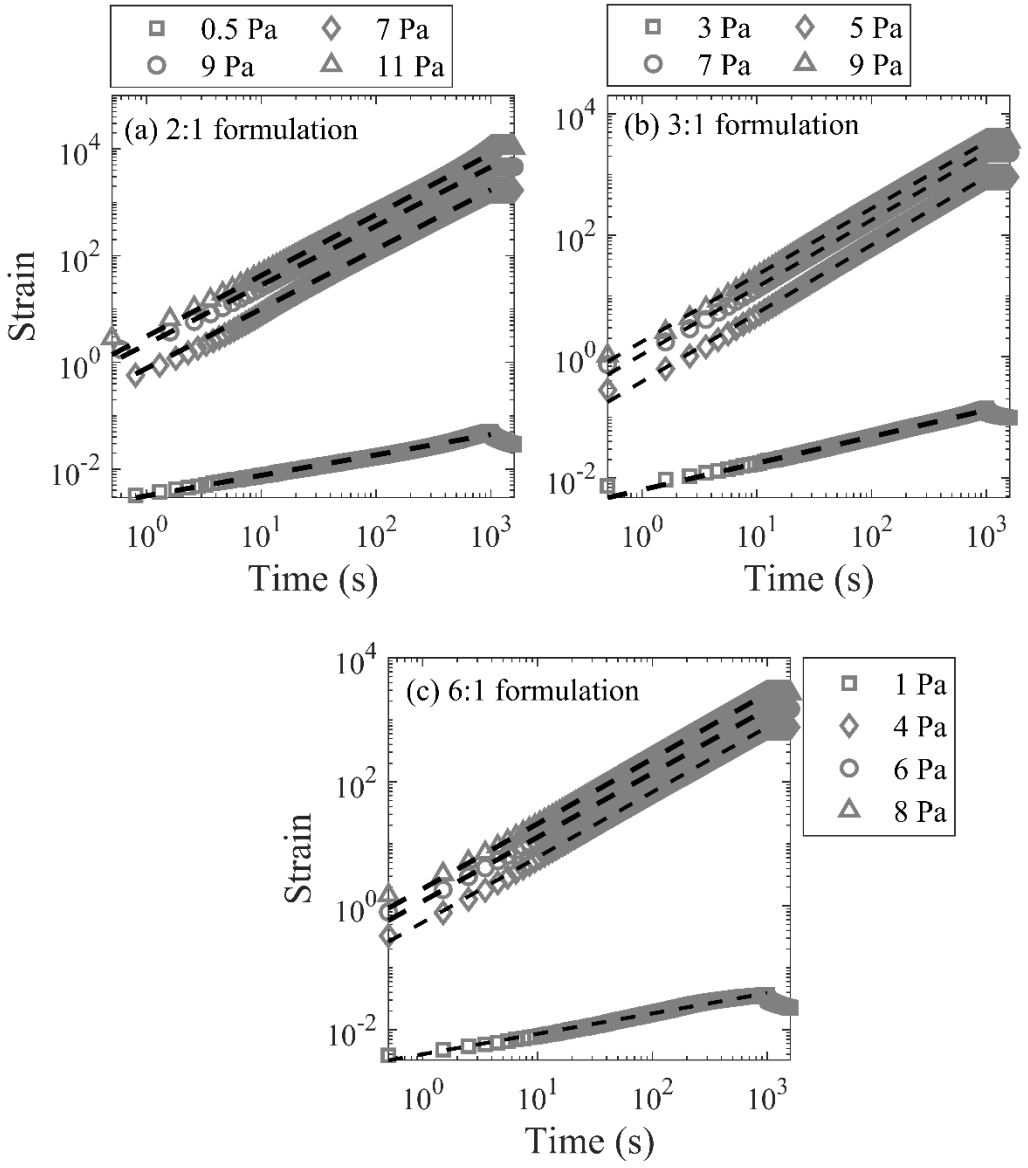

Figure 4. Plots of strain vs time in a creep-recovery test in the (a): 2:1, (b): 3:1 and (c): 6:1 formulations. A constant stress is applied to the fluid for 1000 s before being removed for another 600 s. A transition between elastic behaviour, where some of the strain is recovered, to inelastic behaviour can be seen between 0.5 Pa and 7 Pa in (a), between 3 Pa and 5 Pa in (b) and between 1 Pa and 4 Pa in (c). The power law behaviour of the strain response on either side of the transition in (a), (b) and (c) are approximately the same. The differences in the exact stresses depicted stem from the differences in the yield region in each of the fluids.

$t^{0.329\pm0.005}$ for the 1 Pa case in the 6:1 formulation and $t^{0.437\pm0.003}$ for the 3 Pa case in the 3:1 formulation. Above the bifurcation, this range is $t^{1.035\pm0.002}$ for the 6 Pa case in the 6:1 formulation and $t^{1.125\pm0.004}$ in the 5 Pa case in the 3:1 formulation.

It is unclear what accounts for the strain below the transition point. It is unlikely to be slippage as the plate angular velocity remains below ~10^{-4} $rads^{-1}$ until yielding occurs, similar to the behaviour when there is no torque applied. Additionally, the presence of a lubricating layer would be unlikely to allow recovery of the strain. Behaviour similar to that below the bifurcation was seen by Panizza et al. (1996) in a pure MLV phase sheared at a stress of 0.03 Pa [37]. This, along with the shear thinning data in figure 2 discussed previously, suggests that the fluids are initially in a state dominated by MLVs and that the yield stress can be interpreted as the force required to start moving the MLVs over each other.

3.2 OCT velocimetry

Figure 5 shows how the velocities of the fluids vary with time at a position halfway in the rheometer gap after the onset of shear at a constant stress. The data for the 2:1, 3:1 and 6:1 formulations are shown in figures 5 (a), (b) and (c) respectively. As mentioned previously, the onset of flow is unpredictable in the yield region. However, once flow has begun, the response is repeatable, meaning that velocities at stresses within the yield region can be measured. In all cases, the velocities follow a power law in time of the form t^{β} after a period of transient behaviour during which the velocity can fluctuate. This region is markedly larger for the 2:1 formulation, lasting 50-140 s compared with ~10 s for the 3:1 and 6:1 formulations. It is clear that none of the fluids reach the steady state at the stresses measured and in the time frame of this experiment. Excluding the 15 Pa data and focussing on the data close to the yield region, $\beta < 0.1$, there was no clear pattern relating stress to the exponent. In the case of the 15 Pa data in each formulation, each fluid begins by following a power law with $\beta \approx 0.2$ before transitioning to $\beta = 0.439 \pm 0.004$, $\beta = 0.389 \pm 0.002$, and $\beta = 0.4135 \pm 0.0004$ for (a), (b) and (c) respectively. The 2:1 and 3:1 samples then show an additional change increase in power law to $\beta = 0.702 \pm 0.001$ and $\beta = 0.739 \pm 0.003$ respectively. The time at which each transition occurs increases with the proportion of CTAC in the formulation so it is possible that the 6:1 formulation would undergo the second transition to a power law of $t^{0.7}$ if left for some additional time. Increasing the proportion of CTAC also increases the viscosity measured by the rheometer. For example, the final shear rate recorded in the 2:1 case is $\sim$560 s^{-1}, a figure that drops to $\sim$17 s^{-1} for the 6:1 case. Roux et al. (1993) found that the MLV phase is shear thinning while lamellar phases are Newtonian[36]. If the fluids in this study were Newtonian, that is flowing with a constant viscosity, we would expect the velocity at a specific point in the sample to be constant in time. What we see instead is that the velocity and the shear rate increase with time. This suggests that, if a microstructural change is responsible for the observed transitional behaviour, it is unlikely to be MLVs to lamellae. Another microstructural candidate for this behaviour is the layering transition first described by Diat et al. (1995) where the MLVs are changed from disordered close-packed spherulites to ordered hexagonally-packed layers by shear [39]. The layers slide over each other and Manneville et al. (2004) associate their presence with a reduction in the fluid viscosity [27]. A reduction in the wall slip, as was found to accompany an increased shear rate in figure 7, could also lead to an increased scaling of the velocity. A combination of these factors could be responsible for the two changes in power law seen in the 2:1 and 3:1 cases.

Figure 6 shows velocity profiles collected at constant shear rates between 1 s^{-1} and 150 s^{-1} for each formulation. Figures 6 (a), (c) and (e) show the profiles for 1-20 s^{-1} for the 2:1, 3:1 and 6:1 formulations

respectively, while (b), (d) and (f) show the profiles for 50-150 s^{-1}. In each case, the fluids exhibit plug flow at 1 s^{-1} and 5 s^{-1}, in line with the results observed from 0.01-1 s^{-1} by Datta et al. using particle imaging velocimetry in a lamellar gel network based on BTMS, another cationic surfactant [19]. At rates from 10 s^{-1} to 150 s^{-1}, the fluid appears to show shear banding with three linear regimes indicating constant shear rates, while there is also often a plateau close to the upper plate. In all cases, a slow middle section

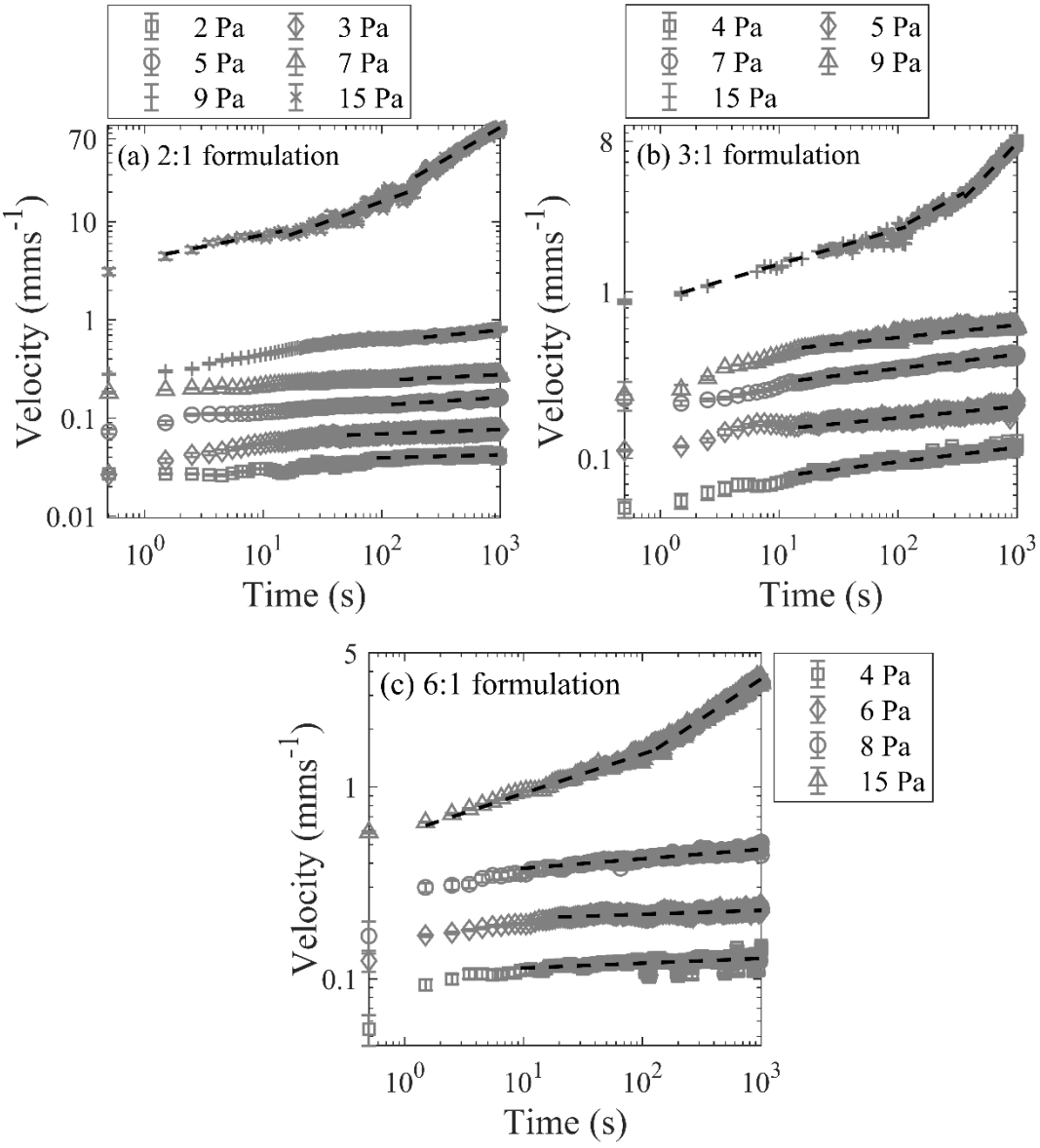

Figure 5. Plots of velocity at a position halfway into the rheometer gap vs time showing the start-up response of the (a) 2:1 sample , (b) 3:1 sample and (c) 6:1 sample to consant stresses. Power law fits are included as dashed lines. At stresses close to the yield region, each plot shows a power law dependence of approximately $t^{<0.1}$ after an initial period of transient fluctuations. In contrast, the plots at 15 Pa show time-dependent transitions from $t^{0.24\pm0.02}$ to $t^{0.439\pm0.004}$, $t^{0.2094\pm0.0006}$ to $t^{0.3886\pm0.002}$ and $t^{0.2044\pm0.0006}$ to $t^{0.4135\pm0.0004}$ in (a), (b) and (c) respectively. There is an additional transition in (a) and (b) from $t^{\sim0.4}$ to $t^{0.702\pm0.001}$and $t^{0.739\pm0.004}$ respectively.

is bounded by two regions with much steeper shear rates. In some cases, the rate in the middle section is so slow it resembles plug flow. This three-band flow structure is seen occasionally in the literature, namely in Bécu et al. (2004) [41] in wormlike micelles, Ravindranath et al. (2008) [23] in entangled polymers, and Medronho et al. (2012) [26] and Manneville et al. (2004) [27] in lamellar phases. In the case of Bécu et al., the three-band structure is a temporary state in response to a fluctuating slip condition at the boundary that causes the third band to nucleate into existence before destructing sporadically. Manneville et al. report a third band in the velocity profile when their fluid is sheared at a constant stress that nucleates near the stator before moving towards the moving side of their Couette geometry. The presence of three bands described by Ravindranath et al. and Medronho et al. are similarly transient, though appear to be distinct stages in a time evolution rather than a result of fluctuations. The results displayed in figure 6 are different to these examples in that they exist consistently over a period of approximately 600 s of shear at a constant rate. This is equivalent to strain values in the tens of thousands for the higher imposed shear rates. In general, the shear rates in the different regions do not follow a pattern based on the ratio of CTAC to fatty alcohol. However, the slow, middle band of the 2:1 formulation appears to be flatter than the other two.

Figure 7 shows how the slip velocity at the upper plate as a fraction of the plate velocity, $\frac{V_{Plate}-V_{Fluid}}{V_{Plate}}$, varies with shear rate in each fluid. In the plug flow regime between $1s^{-1}$ and 5 s^{-1}, the fractional slip velocity shows a plateau at approximately 0.5. Once in the banding regime, from 10 s^{-1} upwards, this decreases significantly with shear rate. Since the bands are stable, it could follow that they would adhere to a variation of the lever rule in equation 1 with three bands. However, a crucial assumption for the application of the lever rule is that the velocity should be continuous at the interfaces. In line with this, a plot of the difference between the applied rate and lever rule sum as a fraction of the applied rate against shear rate follows a similar pattern to figure 7. That is, the lever rule becomes more accurate as the slip decreases. Medronho et al. (2012) associate wall slip in lamellar phases with the presence of MLVs and the absence of slip with aligned layers [26]. This understanding of the microstructural changes occurring in the fluids suggests that the plug flow regime represents a pure MLV state which is replaced by a mixed regime where MLVs and aligned layers coexist once shear banding begins. However, at a given shear rate, the presence of a stable onion phase is typified by an approximately constant viscosity [38]. The data in figure 2 suggests that a transition from MLVs to lamellar sheets is occurring at every measured shear rate. What we see in figure 7 could be understood as the balance shifting from MLVs to lamellar sheets with increasing rate. The formation of MLVs from the initially aligned state is known to be associated with shear thickening, while the pure MLV state is associated with shear thinning [36,61]. The second aligned regime should therefore have a smaller viscosity than the MLV phase, so in a combined state, where shear banding is present, regions of larger shear rate should be associated with aligned lamellae and regions of smaller rate with MLVs [26,28,38]. Applying this logic to the data in figure 6 indicates the presence of two aligned regimes close to either rheometer plate surrounding a central region consisting of mainly MLVs. A diagram showing such a morphology can be seen in figure 8, which shows the MLVs in a hexagonally packed formation. It is impossible to tell whether they are hexagonally packed or close-packed MLVs without additional use of SALS or SANS measurements as performed by Diat et al. (1995) [39]. These measurements aren't possible with the current apparatus, so this figure is purely illustrative rather than definitive.

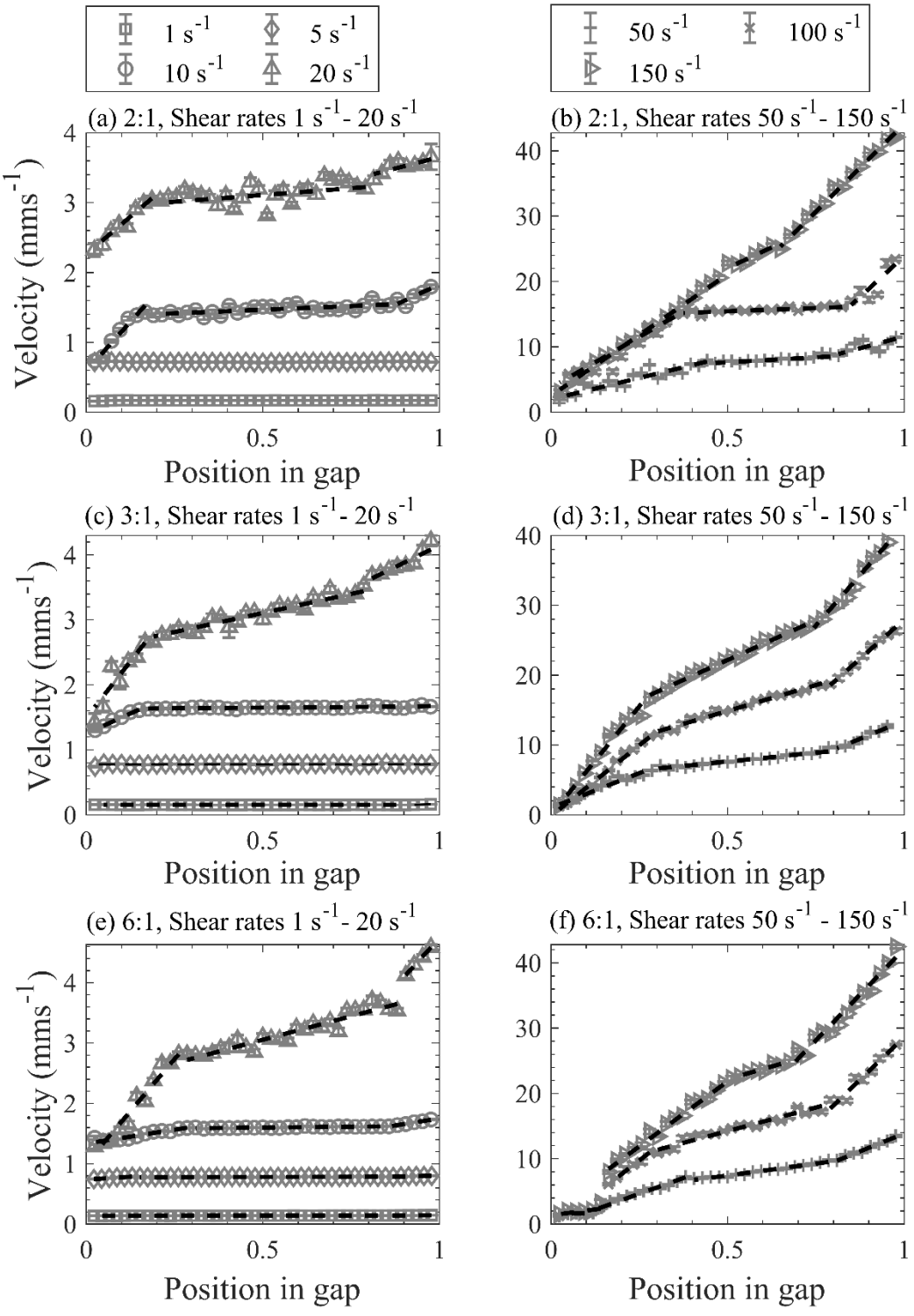

Figure 6. Plots of velocity throughout the rheometer gap at constant shear rates. Plots (a) and (b) show the low and high-rate behaviour for the 2:1 formulation, (c) and (d) show the same thing for the 3:1 formulation and (e) and (f) for the 6:1 formulation. In all cases, at 1 s^{-1} and 5 s^{-1} the fluids show plug flow. At 10 s^{-1} and above, the fluids appear to split into three shear bands, with steep linear gradients close to both surfaces and a shallower region in the middle.

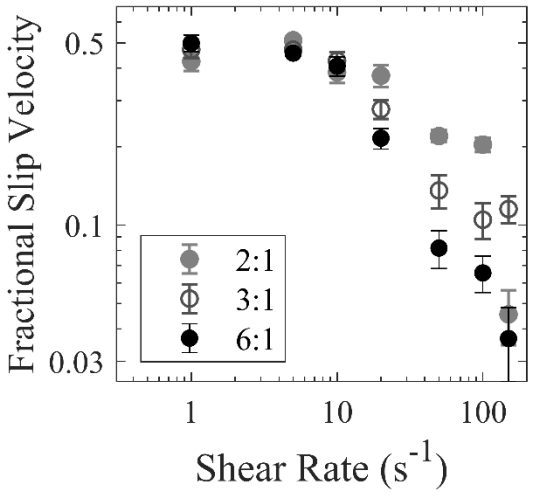

Figure 7. Plot of fractional slip velocity, $\frac{V_{Plate}-V_{Fluid}}{V_{Plate}}$, as a function of shear rate for each formulation. In each case, a plateau exists at rates up to 10 s^{-1} before the slip decreases.

When using OCT velocimetry, the signal originates from within the sample at the point where the optical path length travelled by the light is the same as that in the reference arm of the interferometer. The light in each arm travels through different media, air in the reference arm and the fluid in the sample arm. In our study, the refractive index in the fluid is larger than that of air, so the optical path length is relatively larger, even if the absolute distance it travels is the same. With this knowledge and the assumption that the refractive index is homogeneous throughout the fluid, an estimate for the refractive index can be made from the measured distance the light travels in the sample. Following the method in the supplementary information for Harvey and Waigh (2011) [45], the refractive index of the working fluid in a Michelson OCT apparatus used with a rheometer is given by,

$$n_s = \frac{sin\theta_a}{sin\left(\frac{sin^{-1}(\frac{2x\,sin\,\theta_a}{L_a})}{2}\right)}, \tag{2}$$

where n_s is the sample index, θ_a is the angle between the normal of the rheometer plates and the lens, x is the size of the rheometer gap and L_a is the path length in air that corresponds to the path length travelled through the entirety of the sample. See figure 1 for a visual aid for θ_a and x. Using this formula gives an estimate for the refractive index of the gel network of $1.54 < n_s < 1.66$ for the 2:1 and 3:1 formulations and $1.50 < n_s < 1.79$ for 6:1. In the worst case scenario of a completely oriented sample in the case of the 6:1 formulation, the associated birefringence could thus lead to a 19% error in the position of the bands. However, separate static OCT polarised imaging data implies that the oriented birefringent domain structure is 1-2 orders of magnitude smaller than the rheometer gap size and thus birefringence effects on OCT velocimetry measurements will be substantially smaller due to averaging.

As a relatively new technology, OCT rheometry has never before been used to study opaque lamellar gels and it performs well with both commercial and model formulations. The technique can measure much faster, commercially relevant, shear rates than comparable particle tracking techniques, which is probably why the distinctive 3 banded steady state behaviour has been observed for the first time. An additional advantage of OCT velocimetry over techniques with similar resolution is the relative ease and cheapness of its implementation. This makes it a good candidate for making in-line measurements in an industrial setting. This serves as a key motivation for our investigations into OCT and we are currently working towards directly measuring effects such as wall slip and shear banding on a pipeline. With this motivation in mind, we decided not to use roughened plates to reduce the effects of wall slip as the phenomena is of particular interest.

The use of OCT to measure velocity transients during start up shear has not been previously presented in the literature and provides a new technique to probe phenomena associated with yield stresses. Lamellar gel networks are some of the most challenging rheological materials that exist, since they demonstrate a range of sophisticated non-linear rheological phenomena including thixotropy, shear banding, soft-glassy behaviour, wall slip, and shear thinning. Models of soft glassy rheology show some promise to qualitatively describe some of the phenomena observed [19,62]. It is expected that OCT rheology will find further applications in quantifying the flow behaviour of a wide range of soft glassy materials.

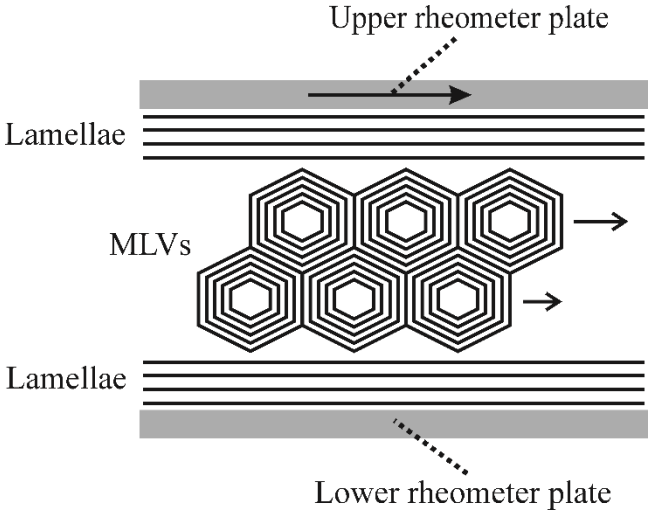

Figure 8. Schematic diagram showing two regions of planar lamellae bounding a centre of hexagonally packed MLVs. The red arrow at the top of the diagram indicates the direction of flow as imposed by the moving upper rheometer plate. The smaller red arrows on the diagram show the MLVs sliding over one another in layers.

4 Conclusions

Lamellar gel networks display a rich variety of robust rheological signatures. Namely, thixotropy and yield stress highlighted in the rheometry data. Through OCT velocimetry, we have directly observed nonlinear flow in our gel network in the form of wall slip and plug flow at rates of ≤5 s^{-1} and shear banding at rates of ≥10 s^{-1}. The three-band structure of the fluids at these rates has been seen previously as a transient

behaviour in complex fluids, but never in the steady state [23,26,27,41]. The form of the rheometry data is characteristic of the type of fluid and, along with the transition from wall slip to shear banding seen via OCT, seems to be indicative of a transition from MLVs to planar lamellae. In addition, the onset of motion associated with the fluid's yield stress was observed directly. The velocity start-up of the fluids was found to follow a power law dependence in time after an initial period of transience. The power law behaviour is weak when the stress is close to the yield region. When the stress is increased, the fluid undergoes two time-dependent transitions to steeper power laws. The origin of this behaviour is unclear but could be related to a transition from disordered to ordered MLVs and the reduction in wall slip at high shear rates.

Competing Interests: The authors declare that they have no competing interests.

Bibliography

[1] T. Iwata, "Lamellar gel network," in *Cosmetic Science and Technology: Theoretical Principles and Applications*, K. Sakamoto, R. Y. Lochhead, H. I. Maibach, and Y. Yamashita, Eds. Elsevier Inc., (2017), 415–447.

[2] H. E. Junginger, "Colloidal structures of O/W creams," *Pharm. Weekbl. Sci. Ed.*, **6**, 141–149, (1984).

[3] G. M. Eccleston, "Functions of mixed emulsifiers and emulsifying waxes in dermatological lotions and creams," *Colloids Surfaces A Physicochem. Eng. Asp.*, **123**–**124**, 169–182, (1997).

[4] R. G. Larson, "Surfactant solutions," in *The Structure and Rheology of Complex Fluids*, 1st ed., Oxford: Oxford University Press, (1999), 359–403.

[5] M. Kranenburg and B. Smit, "Phase behavior of model lipid bilayers," *J. Phys. Chem. B*, **109**, 6553–6563, (2005).

[6] T. E. De Oliveira, F. Leonforte, L. Nicolas-Morgantini, A. L. Fameau, B. Querleux, F. Thalmann, and C. M. Marques, "Fluid bilayer phase in aqueous mixtures of fatty alcohol and cationic surfactant," *Phys. Rev. Res.*, **2**, 013075, (2020).

[7] H. Hoffmann and W. Ulbricht, “Surfactant gels,” *Curr. Opin. Colloid Interface Sci.*, **1**, 726–739, (1996).

[8] H. E. Warriner, S. H. J. Idziak, N. L. Slack, P. Davidson, and C. R. Safinya, “Lamellar biogels: Fluid-membrane-based hydrogels containing polymer lipids,” *Science (80-.).*, **271**, 969–973, (1996).

[9] P. C. F. Møller, J. Mewis, and D. Bonn, “Yield stress and thixotropy: On the difficulty of measuring yield stresses in practice,” *Soft Matter*, **2**, 274–283, (2006).

[10] H. A. Barnes and K. Walters, “The yield stress myth?,” *Rheol. Acta*, **24**, 323–326, (1985).

[11] P. Coussot, Q. D. Nguyen, H. T. Huynh, and D. Bonn, “Viscosity bifurcation in thixotropic, yielding fluids,” *J. Rheol. (N. Y. N. Y).*, **46**, 573–589, (2002).

[12] D. Bonn, M. M. Denn, L. Berthier, T. Divoux, and S. Manneville, “Yield stress materials in soft condensed matter,” *Rev. Mod. Phys.*, **89**, 03005, (2017).

[13] C. Tiu and D. V. Boger, “Complete rheological characterization of time-dependent food products,” *J. Texture Stud.*, **5**, 329–338, (1974).

[14] D. De Kee, R. K. Code, and G. Turcotte, “Flow Properties of Time-Dependent Foodstuffs,” *J. Rheol. (N. Y. N. Y).*, **27**, 581–604, (1983).

[15] K. Dullaert and J. Mewis, “A structural kinetics model for thixotropy,” *J. Nonnewton. Fluid Mech.*, **139**, 21–30, (2006).

[16] P. Sollich, F. Lequeux, P. Hébraud, and M. E. Cates, “Rheology of Soft Glassy Materials,” *Phys. Rev. Lett.*, **78**, 2020–2023, (1997).

[17] R. G. Larson and Y. Wei, “A review of thixotropy and its rheological modeling,” *J. Rheol. (N. Y. N. Y).*, **63**, 477–501, (2019).

[18] J. R. Stokes and J. H. Telford, “Measuring the yield behaviour of structured fluids,” *J. Nonnewton. Fluid Mech.*, **124**, 137–146, (2004).

[19] A. Datta, V. S. Tanmay, G. X. Tan, G. W. Reynolds, S. N. Jamadagni, and R. G. Larson, “Characterizing the rheology, slip, and velocity profiles of lamellar gel networks,” *J. Rheol. (N. Y. N. Y).*, **64**, 851–862, (2020).

[20] S. Lerouge and J. F. Berret, “Shear-induced transitions and instabilities in surfactant wormlike micelles,” in *Polymer Characterization. Advances in Polymer Science, vol 230.*, K. Dusek and J. Joanny, Eds. Berlin, Heidelberg: Springer, (2010).

[21] M. P. Lettinga and S. Manneville, “Competition between Shear Banding and Wall Slip in Wormlike Micelles,” *Phys. Rev. Lett.*, **103**, 248302, (2009).

[22] J. B. Salmon, A. Colin, S. Manneville, and F. Molino, “Velocity Profiles in Shear-Banding Wormlike Micelles,” *Phys. Rev. Lett.*, **90**, 228303, (2003).

[23] S. Ravindranath, S. Q. Wang, M. Olechnowicz, and R. P. Quirk, “Banding in simple steady shear of entangled polymer solutions,” *Macromolecules*, **41**, 2663–2670, (2008).

[24] A. Malm, T. A. Waigh, S. Jaradat, and R. Tomlin, “Optical Coherence Tomography Velocimetry with complex fluids,” in *Journal of Physics: Conference Series*, (2015), **602**, 012039.

[25] S. Jaradat, M. Harvey, and T. A. Waigh, “Shear-banding in polyacrylamide solutions revealed via optical coherence tomography velocimetry,” *Soft Matter*, **8**, 11677–11686, (2012).

[26] B. Medronho, U. Olsson, C. Schmidt, and P. Galvosas, “Transient and steady-state shear banding in a lamellar phase as studied by rheo-NMR,” *Zeitschrift fur Phys. Chemie*, **226**, 1293–1313, (2012).

[27] S. Manneville, J. B. Salmon, and A. Colin, “A spatio-temporal study of rheo-oscillations in a

sheared lamellar phase using ultrasound," *Eur. Phys. J. E Soft Matter*, **13**, 197–212, (2004).

[28] J. B. Salmon, S. Manneville, and A. Colin, "Shear banding in a lyotropic lamellar phase. I. Time-averaged velocity profiles," *Phys Rev E Stat Nonlin Soft Matter Phys.*, **68**, 051503, (2003).

[29] G. M. H. Wilkins and P. D. Olmsted, "Vorticity banding during the lamellar-to-onion transition in a lyotropic surfactant solution in shear flow," *Eur. Phys. J. E*, **21**, 133–143, (2006).

[30] P. Coussot, J. S. Raynaud, F. Bertrand, P. Moucheront, J. P. Guilbaud, H. T. Huynh, S. Jarny, and D. Lesueur, "Coexistence of liquid and solid phases in flowing soft-glassy materials," *Phys. Rev. Lett.*, **88**, 218301, (2002).

[31] A. Raudsepp and P. T. Callaghan, "A rheo-optical study of shear rate and optical anisotropy in wormlike micelles solutions," *Soft Matter*, **4**, 784–796, (2008).

[32] K. W. Feindel and P. T. Callaghan, "Anomalous shear banding: Multidimensional dynamics under fluctuating slip conditions," *Rheol. Acta*, **49**, 1003–1013, (2010).

[33] S. Kuczera, C. Perge, M. A. Fardin, T. I. Brox, M. A. K. Williams, S. Manneville, and P. Galvosas, "Anomalous shear banding revisited with Rheo-NMR and Rheo-USV," *Rheol. Acta*, **54**, 619–636, (2015).

[34] S. Manneville, J. B. Salmon, L. Bécu, A. Colin, and F. Molino, "Inhomogeneous flows in sheared complex fluids," *Rheol. Acta*, **43**, 408–416, (2004).

[35] O. Diat, D. Roux, and F. Nallet, "Effect of shear on a lyotropic lamellar phase," *J. Phys. II, EDP Sci.*, **3**, 1427–1452, (1993).

[36] D. Roux, F. Nallet, and O. Diat, "Rheology of Lyotropic Lamellar Phases," *Eur. Lett.*, **24**, 53–58, (1993).

[37] P. Panizza, D. Roux, V. Vuillaume, C.-Y. D. Lu, and M. E. Cates, “Viscoelasticity of the Onion Phase,” *Langmuir*, **12**, 248–252, (1996).

[38] C. Oliviero, L. Coppola, R. Gianferri, I. Nicotera, and U. Olsson, “Dynamic phase diagram and onion formation in the system C 10E3/D2O,” *Colloids Surfaces A Physicochem. Eng. Asp.*, **228**, 85–90, (2003).

[39] O. Diat, D. Roux, and F. Nallet, “‘Layering’ effect in a sheared lyotropic lamellar phase,” *Phys. Rev. E Stat Phys Plasmas Fluids Relat Interdiscip Top.*, **51**, 3296–3300, (1995).

[40] T. Divoux, C. Barentin, and S. Manneville, “Stress overshoot in a simple yield stress fluid: An extensive study combining rheology and velocimetry,” *Soft Matter*, **7**, 9335–9349, (2011).

[41] L. Bécu, S. Manneville, and A. Colin, “Spatiotemporal dynamics of wormlike micelles under shear,” *Phys. Rev. Lett.*, **93**, 018301, (2004).

[42] B. Medronho, J. Brown, M. G. Miguel, C. Schmidt, U. Olsson, and P. Galvosas, “Planar lamellae and onions: A spatially resolved rheo-NMR approach to the shear-induced structural transformations in a surfactant model system,” *Soft Matter*, **7**, 4938–4947, (2011).

[43] B. Medronho, S. Shafaei, R. Szopko, M. G. Miguel, U. Olsson, and C. Schmidt, “Shear-induced transitions between a planar lamellar phase and multilamellar vesicles: Continuous versus discontinuous transformation,” *Langmuir*, **24**, 6480–6486, (2008).

[44] A. V. Malm, A. W. Harrison, and T. A. Waigh, “Optical coherence tomography velocimetry of colloidal suspensions,” *Soft Matter*, **10**, 8210–8215, (2014).

[45] M. Harvey and T. A. Waigh, “Optical coherence tomography velocimetry in controlled shear flow,” *Phys. Rev. E - Stat. Nonlinear, Soft Matter Phys.*, **83**, 031502, (2011).

[46] C. Casugbo, M. Flanagan, J.A. Hough, J.M. Naughton, and D. Serridge, "Composition", European

Patent Office, Patent No. EP 2877144, (2014).

[47] G. E. Cunningham, F. Alberini, M. J. H. Simmons, and J. J. O'Sullivan, "Understanding the effects of processing conditions on the formation of lamellar gel networks using a rheological approach," *Chem. Eng. Sci.*, **242**, 116752, (2021).

[48] D. Huang, E. a Swanson, C. P. Lin, J. S. Schuman, W. G. Stinson, W. Chang, M. R. Hee, T. Flotire, K. Gregory, C. a Puliafito, and J. G. Fujimoto, "Optical Coherence Tomography," *Science (80-.).*, **254**, 1178–1181, (1991).

[49] A. F. Fercher, W. Drexler, C. K. Hitzenberger, and T. Lasser, "Optical coherence tomography - principles and applications," *Rep. Prog. Phys.*, **66**, 239–303, (2003).

[50] X. J. Wang, T. E. Milner, and J. S. Nelson, "Characterization of fluid flow velocity by optical Doppler tomography," *Opt. Lett.*, **20**, 1337–1339, (1995).

[51] Z. Chen, T. E. Milner, D. Dave, and J. S. Nelson, "Optical Doppler tomographic imaging of fluid flow velocity in highly scattering media," *Opt. Lett.*, **22**, 64–66, (1997).

[52] A. V. Malm and T. A. Waigh, "Elastic turbulence in entangled semi-dilute DNA solutions measured with optical coherence tomography velocimetry," *Sci. Rep.*, **7**, 1186, (2017).

[53] R. Leitgeb, C. Hitzenberger, and A. Fercher, "Performance of fourier domain vs time domain optical coherence tomography," *Opt. Express*, **11**, 889–894, (2003).

[54] M. A. Choma, M. V. Sarunic, C. Yang, and J. A. Izatt, "Sensitivity advantage of swept source and Fourier domain optical coherence tomography," *Opt. Express*, **11**, 2183–2189, (2003).

[55] X. Zhu, Y. Liang, Y. Mao, Y. Jia, Y. Liu, and G. Mu, "Analyses and calculations of noise in optical coherence tomography systems," *Front. Optoelectron. China*, **1**, 247–257, (2008).

[56] E. Brown and H. M. Jaeger, “Shear thickening in concentrated suspensions: Phenomenology, mechanisms and relations to jamming,” *Reports Prog. Phys.*, **77**, 046602, (2014).

[57] J. Mewis and N. J. Wagner, “Thixotropy,” *Advances in Colloid and Interface Science*, **147**–**148**. 214–227, Mar. 2009.

[58] S. M. Fielding, P. Sollich, and M. E. Cates, “Aging and rheology in soft materials,” *J. Rheol. (N. Y. N. Y).*, **44**, 323–369, (2000).

[59] P. Sollich, “Soft Glassy Rheology,” in *Molecular Gels*, R. G. Weiss and P. Terech, Eds. Dordrecht: Springer, (2006), 161–192.

[60] D. Sornette, *Critical Phenomena in Natural Sciences*, 2nd ed. Berlin, Heidelberg: Springer, (2006).

[61] S. Müller, C. Börschig, W. Gronski, C. Schmidt, and D. Roux, “Shear-induced states of orientation of the lamellar phase of C12E4/water,” *Langmuir*, **15**, 7558–7564, (1999).

[62] F. Wang and R. G. Larson, “Thixotropic constitutive modeling of shear banding by boundary-induced modulus gradient in lamellar gel networks,” *J. Rheol. (N. Y. N. Y).*, **67**, 35–51, (2023).